RSC Advances

PAPER

View Article Online
View Journal | View Issue

Cite this: *RSC Adv.*, 2025, **15**, 19034

Tandem catalysis of zeolite and perovskite for light olefins production in dehydrogenation cracking of naphtha†

Songlu Yao, Jianhong Gong,* Xiaoqiao Zhang,* Xiaoli Wei, Di Wang and Tengwei Chen

Considerable energy consumption and high CO_2 emissions of steam cracking have driven the exploration of alternative methods for light olefins production from naphtha. In this context, we propose a novel dehydrogenation cracking approach as an alternative route for naphtha conversion. By employing a perovskite-based redox catalyst, $CaMnO_3$@Na_2WO_4, in combination with zeolite-based catalyst, model compound *n*-octane undergoes dehydrogenation to form octene, significantly reducing the activation energy required for C–C bond cleavage. This approach enhances the yield and selectivity of light olefins. When mixing ratio of dehydrogenation catalyst in tandem catalysis is 5%, the conversion reaches 90.07%, and the total light olefins yield is 47.90%. The influence of factors such as reaction temperature, coupling mode and mixing ratio were also demonstrated. Comparing to standalone zeolites, 15% higher olefin yields were obtained with tandem mixed catalysts, demonstrating the excellent dehydrogenation cracking ability. The optimized dehydrogenation temperature at 450 °C, could provide an optimal reaction environment for this elementary dehydrogenation reaction and decrease the energy consumption. Synergetic effect of zeolite-based catalyst with different mixing ratio of $CaMnO_3$@Na_2WO_4 also leads to tunable P/E ratio. Theoretical calculations of reaction routes provided valuable insights for the further development and optimization of naphtha conversion processes.

Received 8th April 2025
Accepted 26th May 2025

DOI: 10.1039/d5ra02427g

rsc.li/rsc-advances

1 Introduction

As fundamental building blocks in the petrochemical industry, light olefins such as ethylene and propylene are valuable feedstocks to produce polymers, oxygenates, and various other chemical products.[1] In recent years, the demand for ethylene and propylene in the market has been steadily increasing.[2] The steam cracking of naphtha is the primary technology for the production of ethylene and propylene.[3] Recent studies highlight development of olefin polymerization process and offer sustainable routes for olefin production.[4–12] However, the high energy consumption and CO_2 emissions associated with steam cracking necessitate the exploration of alternative methods for producing light olefins from naphtha.[13] Furthermore, the goals of carbon peaking and carbon neutrality in China have placed pressure on the refining industry to transform from a fuel-based to a chemical-based model[14,15]

In comparison to conventional steam cracking, the oxidative dehydrogenation (ODH) represents a promising alternative due to the exothermicity of the reaction and its potential to achieve high single-pass conversion.[16,17] However, the expensive air separation step and safety concerns arising from the co-feeding of hydrocarbons and oxygen make ODH challenging to implement on an industrial scale.[18] To address these limitations, chemical looping oxidative dehydrogenation (CL-ODH) has been proposed as a solution.[19] Unlike steam cracking and conventional ODH, CL-ODH can operate autothermally, eliminating the need for low-temperature air separation and preventing direct contact between hydrocarbons and oxygen. In CL-ODH, a redox catalyst is continuously circulated between two reactors. The redox catalyst serves as the oxygen carrier and donates its lattice oxygen to convert hydrogen from dehydrogenation reaction into water, resulting in favorable light olefins yield.

The selection of oxygen carriers is one of the most important factors for good performance of ODH process. The advantages of perovskite-based metal oxides include their structural flexibility and compositional versatility to accommodate significant oxygen vacancies at relatively low operating temperatures.[20,21] $CaMnO_3$-based perovskite materials are promising options in ODH processes. Alberto Abad and coworkers have explored the thermochemical properties of $CaMnO_3$-based material for a better prediction of non-stoichiometry δ, which is a function of temperature and oxygen partial pressure.[22] Na_2WO_4-

Research Institute of Petroleum Processing Co., Ltd, SINOPEC, 18 Xueyuan Road, Beijing 100083, PR China. E-mail: gongjh.ripp@sinopec.com; xqiaozhang@foxmail.com

† Electronic supplementary information (ESI) available. See DOI: https://doi.org/10.1039/d5ra02427g

promoted $CaMnO_3$ showed steady selective hydrogen combustion (SHC) performance in CL-ODH of ethane with 89% H_2 conversion and 88% selectivity at 850 °C over 50 redox cycles. 0.5 wt% Rh promoted $CaMnO_3$ achieved over 80% syngas selectivity at 600 °C from methane partial oxidation.[23,24] Despite multitude of studies demonstrating the capability of various $CaMnO_3$-based materials,[25–28] systematic studies on dehydrogenation cracking of naphtha with promoted $CaMnO_3$, have yet to be performed.

Dehydrogenation cracking of naphtha, which combines catalytic dehydrogenation and cracking reactions, is a promising approach to reduce the energy consumption and carbon emissions in the production of light olefins from naphtha. By the use of a dehydrogenation catalyst such as Pt–Sn/Ca–$ZnAl_2O_4$ prior to cracking, yields of ethylene and propylene were improved over those obtained by using rare earth-loaded cracking catalyst.[29] It was found that the dehydrogenation cracking reaction effectively proceeds by the tandem reaction. The hydrogen atoms of the alkane first interact with the metal sites of the dehydrogenation catalyst, promoting the dissociation of C–H bonds to form hydrogen and alkenes.[30] Subsequently, the cracking catalyst selectively catalyzes the cracking of the olefins. Since the activation energy for the C–H and C–C bond cleavage during alkenes catalytic cracking is lower than that of alkanes, this process enhances the yield and selectivity of light olefins.

In the current study, a highly selective redox perovskite catalyst, $CaMnO_3$@Na_2WO_4, was employed in the oxidative dehydrogenation reaction. Furthermore, $CaMnO_3$@Na_2WO_4 was coupled with zeolite-based catalysts. Fixed bed experiments were performed to confirm the synergetic effect of zeolite-perovskite composites for enhanced production of light olefins. *n*-Octane was used as a model compound for dehydrogenation cracking of naphtha. The effects of reaction temperature, coupling mode, and mixing ratio on the reaction were investigated in detail. Theoretical calculations of reaction path and modified reaction parameters were also proposed.

2 Experimental

2.1 Materials

$CaMnO_3$ was synthesized using the modified Pechini method. To synthesize $CaMnO_3$, a certain stoichiometric amount of $Mn(NO_3)_2 \cdot 4H_2O$ and $Ca(NO_3)_2 \cdot 4H_2O$ was dissolved in deionized water and stirred for 30 min, and then citric acid was added to the solution with the metal ions (Mn^{2+} and Ca^{2+}) in a molar ratio of 3 : 1. The mixture was stirred at 500 rpm for 30 min. Then, ethylene glycol and citric acid in a molar ratio of 2 : 1 were added to the mixture to promote gel formation. The solution was heated to 80 °C with constant stirring until a viscous gel was formed, and then the beaker was dried in an oven at 120 °C overnight.[31] The dried precursors were first pretreated in a muffle furnace at 450 °C for one hour to burn off the nitrate and then calcined in a tube furnace at 1000 °C with an airflow of about 100 mL min^{-1} for ten hours.

Promotion of the as-obtained $CaMnO_3$ materials with 20 wt% Na_2WO_4 was done by wet impregnation. Finally, the sample $CaMnO_3$@Na_2WO_4 were calcined at 1000 °C for eight hours under air. All the catalysts were sieved in the size range 300–425 μm and used for the reaction tests.

The commercial zeolite-based MMC catalysts were obtained from Sinopec Catalyst Co., Ltd (Beijing, China), with 30 wt% of HZSM-5 zeolite (Si/Al ratio = 21) as an active component. $Mn(NO_3)_2 \cdot 4H_2O$, $Ca(NO_3)_2 \cdot 4H_2O$, ethylene glycol, and citric acid were purchased from Aladdin Reagent Co. Ltd (Shanghai, China).

2.2 Characterization

The crystallinity of catalysts was determined using a D5005 X-ray diffractometer manufactured by Siemens, Germany. The N_2 adsorption–desorption experiments were carried out using an automatic adsorption meter, model ASAP2420, manufactured by Micro metric Instruments, USA, and the specific surface area and pore volume were calculated using the Brunauer–Emmett–Teller (BET) equation. The transmission electron microscopy (TEM, Tecnai G2 F20) was conducted using the field emission transmission electron microscope that was manufactured by FEI Company. The elemental composition of the catalyst was measured using an inductively coupled plasma optical emission spectrometer (ICP-OES) on an Agilent 720 instrument, USA.

2.3 Catalytic performance test

A fixed-bed reactor was used for the dehydrogenation reaction and dehydrogenation cracking reaction. Standalone $CaMnO_3$@Na_2WO_4 perovskite was employed in dehydrogenation reaction. $CaMnO_3$@Na_2WO_4 and zeolite-based MMC catalysts were mixed in physical or tandem mode in dehydrogenation cracking reaction. Before the reaction, the whole system was purged with N_2. When feeding, the reactants were diluted with N_2, preheated to 150 °C, and then injected into the reactor. The reaction temperatures were set at different reaction temperatures. The products were separated into gas and liquid phases by a cooling bath (−19 °C). The gas phase products were analyzed using an online gas chromatograph model GC7890A from Agilent, USA, and the mass of the gas phase was calculated using the ideal gas equation. The liquid phase products were analyzed using an off-line gas chromatograph model 7890B from Agilent, USA. Moreover, the fixed-bed reaction could be divided into two stages, which makes the separated reaction temperatures possible.

2.4 Computational studies

DFT calculations were performed using the $DMol^3$ software developed by Accelrys Inc. The geometries of the metal oxide and zeolite cluster models used in this work were obtained from the framework structure obtained from Material Studio 2019. Relativistic effects were taken into account using an all-electron scalar relativistic method. All calculations were performed using the DNP basis set. The convergence criteria (energy, force, and displacement) were set at 0.05 kJ mol^{-1}, 10^{12} N, and 5×10^{-13} m, respectively.

Table 1 BET specific surface area, pore size, and pore volume of $CaMnO_3$@Na_2WO_4 catalyst

BET surface area/$m^2\ g^{-1}$	Pore volume/($cm^3\ g^{-1}$)	Mesopore volume/($cm^3\ g^{-1}$)	Micropore volume/($cm^3\ g^{-1}$)	Average pore size/nm
2.81	0.006	0.006	0.0002	8.53

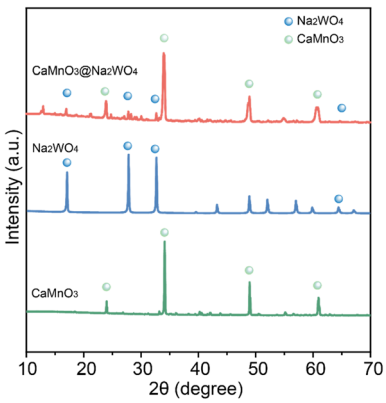

Fig. 1 XRD patterns of perovskite metal oxides $CaMnO_3$ and $CaMnO_3$@Na_2WO_4.

3 Results and discussion

3.1 Physical and chemical structure of catalysts

As shown in Table 1, the specific surface area of the perovskite dehydrogenation catalyst is 2.81 $m^2\ g^{-1}$. The catalyst material does not provide high pore volume. The average pore size is 8.53 nm.

As shown in Fig. 1, the XRD patterns showed the characteristic peaks of $CaMnO_3$ phases in both samples. The characteristic peaks of the Na_2WO_4 were also observed in the $CaMnO_3$@Na_2WO_4 sample, confirming its successful synthesis.

$CaMnO_3$ was synthesized using the modified Pechini method. The Pechini process calls for forming a chelate between mixed cations (dissolved as salts in a water solution) with a hydroxycarboxylic acid (citric acid is preferred). The cations are chelated and then, with the aid of polyalcohols, the chelates are cross-linked to create a gel through esterification. This has the distinct advantage of allowing the use of metals that do not have stable hydroxo species. This method has been extensively applied toward the synthesis of a variety of multicomponent oxides. All the studies reported have clearly indicated that the Pechini method is quite suitable for producing highly pure and homogeneous oxides at reduced temperatures.[32]

The morphologies of $CaMnO_3$@Na_2WO_4 catalyst was examined by transmission electron microscopy in Fig. 2. As indicated by TEM, Na_2WO_4 promotion on $CaMnO_3$ forms a core–shell structure. Surface enrichment of Na_2WO_4 was shown to have a significant suppression effect on surface cation and oxygen species,[33,34] which resulted in greater olefin selectivity and improved yields.

3.2 Theoretical thermodynamic analysis of *n*-octane dehydrogenation reaction

From the perspective of thermodynamics, the reaction equilibrium of octane dehydrogenation reaction was calculated in Table 2. Methane appeared at temperatures above 600 °C, as a symbolic product of thermal cracking reaction. Different ratios of alkanes/alkenes were obtained at various temperature. It could be observed that thermal cracking happened from 600 °C, and reaction rates increased above this temperature. To avoid thermal cracking, dehydrogenation temperature should be kept under 600 °C. More discussion will be added with the following experimental data together.

The thermodynamics calculation of *n*-octane dehydrogenation reaction conversion was showed in Fig. 3. The conversion increases with reaction temperature, and the equilibrium conversion achieved 90% when reaction temperature above 600 °C. The dehydrogenation reaction of long-chain alkanes is not limited by thermodynamic equilibrium at high temperatures. For the endothermic reaction of alkane dehydrogenation, ΔH does not change much with the temperature increase. The equilibrium constants for the dehydrogenation reactions of *n*-octane to form straight-chain olefin were small. Temperature is a sensitive thermodynamic parameter, and the equilibrium conversion of *n*-octane shows a significant increase with reaction temperature. Octene is thermodynamically unstable, and the dehydrogenation of octane is quickly followed by further dehydrogenation and cyclization.

3.3 $CaMnO_3$@Na_2WO_4 perovskite for *n*-octane dehydrogenation reaction

A series of tests were conducted to assess the applicability of the redox catalyst to *n*-octane dehydrogenation reaction and the

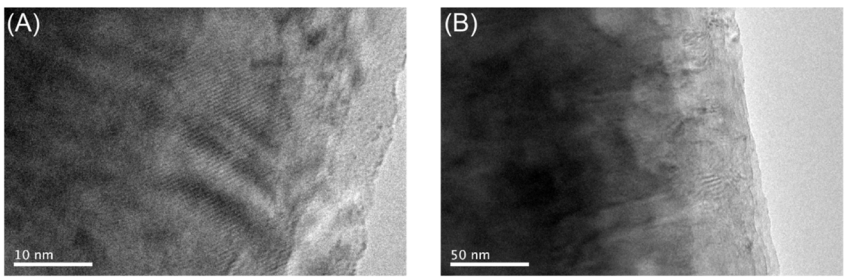

Fig. 2 TEM images of $CaMnO_3$@Na_2WO_4. (A) 10 nm, (B) 50 nm.

Table 2 Theoretical thermodynamic calculation of *n*-octane dehydrogenation reaction equilibrium

Temperature (°C)	350	400	450	500	550	600	650
H_2	0.001	0.003	0.007	0.011	0.014	0.016	0.018
CH_4	0.000	0.000	0.000	0.000	0.000	0.003	0.010
C_2H_2	0.000	0.000	0.000	0.000	0.000	0.000	0.000
C_2H_4	0.000	0.000	0.000	0.001	0.006	0.033	0.124
C_2H_6	0.000	0.000	0.000	0.000	0.001	0.007	0.027
C_3=	0.000	0.000	0.000	0.000	0.003	0.016	0.059
C_3	0.000	0.000	0.000	0.000	0.000	0.000	0.000
C_4–C_6	0.000	0.000	0.000	0.001	0.005	0.025	0.083
Aromatics	0.000	0.000	0.000	0.000	0.002	0.017	0.074
Octane	0.917	0.806	0.615	0.375	0.180	0.073	0.022
Octene	0.082	0.190	0.378	0.612	0.788	0.810	0.584

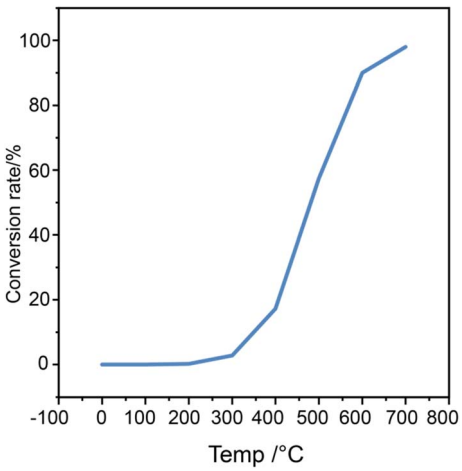

Fig. 3 Thermodynamics calculation of *n*-octane dehydrogenation reaction conversion.

resulting product distributions. The dehydrogenation reaction was carried out on a fixed-bed micro-reactor device using $CaMnO_3$@Na_2WO_4 as the dehydrogenation catalyst and *n*-octane as the raw material. Fig. 4 illustrates the relationships between *n*-octane conversion and reaction temperature. The redox catalyst serves as the oxygen carrier and donates its lattice oxygen to oxidation reaction with hydrogen, resulting in favorable ethylene and propylene yields.[34] It is observed that the conversion of *n*-octane significantly increases with higher reaction temperature. At 500 °C, the dehydrogenation conversion was only 6.8% due to the relatively low reaction temperature. However, as the temperature increased, the conversion improved significantly, reaching 42.9% at 675 °C. This indicates that the activity and selectivity of oxygen species in the $CaMnO_3$@Na_2WO_4 catalysts are highly temperature dependent. At higher temperatures, more lattice oxygen is transported to the redox catalyst surface at higher rates. This leads to increased active oxygen species on the redox catalyst surface for higher conversion.[33] The redox catalyst serves as the oxygen carrier and donates its lattice oxygen to convert hydrogen from *n*-octane dehydrogenation into water, resulting in favorable light olefins yields.

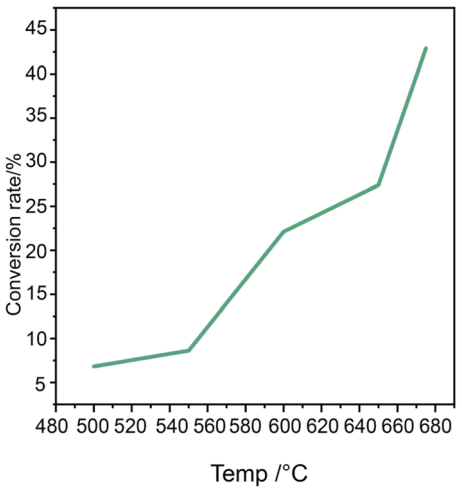

Fig. 4 Effect of reaction temperature on the conversion of the *n*-octane dehydrogenation reaction with $CaMnO_3$@Na_2WO_4 perovskite.

Dehydrogenation of *n*-octane is an endothermic reaction. Higher temperature is beneficial for C–H bonds cleavage and the following H_2 combustion, promoting the conversion of *n*-octane. *n*-Octane undergoes catalytic cracking with acid active sites on zeolites and forms light olefins and hydrogen in the gas phase. The hydrogen is then combusted on the gas-molten Na_2WO_4 interface to form water under a redox scheme. The removal of H_2 can increase *n*-octane conversions by shifting the cracking reaction equilibrium. The addition of Na_2WO_4 on $CaMnO_3$ allows the H_2 combustion to occur at the gas-molten shell interface by the lattice oxygen transported by WO_4^{2-} which undergoes WO_3^- and WO_4^{2-} transition.[33,34]

Effect of reaction temperatures on the yields of ethylene and propylene in *n*-octane dehydrogenation reaction was presented in Fig. 5. The detailed production distribution was presented in Table 3. With the gradual increase in reaction temperature, the yield of ethylene and propylene in *n*-octane dehydrogenation reaction products increased. At 500 °C, yields of ethylene and propylene were 1% and 0.9%, respectively. At 700 °C, the ethylene and propylene yields were 13.1% and 6.5%, respectively. Octene, as one component in gasoline product, is thermodynamically unstable. It trends to crack into smaller molecules at high temperature. The yields of octene decreased from 0.83% to 0.43%, when reaction temperature increased from 500 °C to 700 °C. The carbon balance was calculated to be 95–103%.

As reported by Gao *et al.*, the olefin yield is below 2% at 550 °C with *n*-hexane as feedstock.[35] This is consistent with our results. A standalone redox catalyst requires high operating temperature (>750 °C) to exhibit satisfactory olefin yields. Na_2WO_4 modifies the oxygen donation behavior of $CaMnO_3$ and provides a catalytically active surface. The oxygen species were transported through the molten Na_2WO_4 layer to participate in oxidative dehydrogenation.[36] Melting point of Na_2WO_4 is 698 °C.

As shown in Fig. 6, octene selectivity decreases continuously with temperature, with 9% octene selectivity at 500 °C and 1% at 675 °C. This could be attributed that octene is very thermodynamically unstable and highly susceptible to cracking reactions

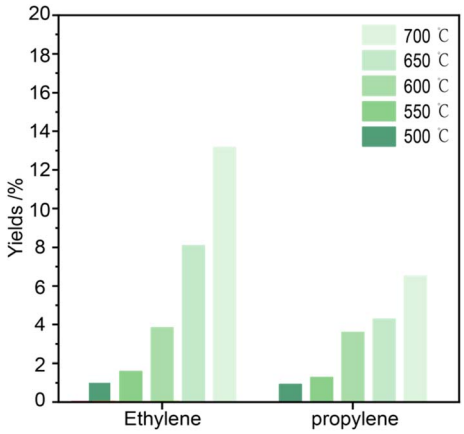

Fig. 5 Effect of reaction temperatures on the yields of ethylene and propylene in *n*-octane dehydrogenation reaction with $CaMnO_3$@Na_2WO_4.

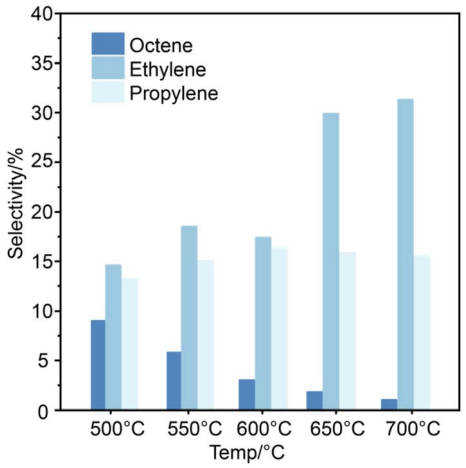

Fig. 6 Effect of different reaction temperatures on selectivity of *n*-octane dehydrogenation reaction products.

at high temperature. This is consistent with the previous thermodynamic calculations. The propylene selectivity does not vary much with temperature. The ethylene selectivity is highest at 700 °C with 31.3%. Lower operating temperatures have the effect of lowering the oxygen capacity of the redox catalyst.

3.4 Synergetic effect of dehydrogenation and cracking active sites

Due to the relatively stable structure of *n*-octane and the high C–C bond energy, the reaction temperature required for the catalytic conversion of *n*-octane with perovskite catalysts is usually above 700 °C.[34] To lower the required reaction temperature, the dehydrogenation catalyst could be coupled with zeolite cracking catalysts. In our previous study, *n*-octane is firstly dehydrogenated at the dehydrogenation site, and the resulting octene is cracked at the acidic site of zeolite catalysts, which improves the conversion and olefin selectivity of *n*-octane.[37] In this study, two common coupling methods, directly mechanical mixing and tandem mixing were chosen to compare the different effects.

Tandem catalysis continues to expand the realm of heterogeneous catalysis in enabling sustainable alternatives for chemical and fuel production. Typically, it provides promising alternatives to circumvent the thermodynamic challenge of direct dehydrogenation of light alkanes as an on-purpose route for olefin production *via* coupling dehydrogenation and cracking active sites.[37] As shown in Fig. 7, for the *n*-octane dehydrogenation cracking reaction, the dehydrogenation catalyst was mechanically or tandem mixed with the cracking catalyst. The different ratios of dehydrogenation catalysts include 1%, 3% and 5%. Both coupling methods show conversion of *n*-octane that was consistently lower than the cracking background (given by the dashed line). The conversion increased with the proportion of dehydrogenation catalyst, but it was lower than that of the cracking reaction alone. When 5% dehydrogenation catalyst was added and mechanically mixed with the cracking catalyst, the conversion was 86.1%. When 5% dehydrogenation catalyst was tandem mixed, the conversion was 90.7%.

As shown in Fig. 8, after physical mixing of $CaMnO_3$@Na_2WO_4 dehydrogenation catalyst and zeolite-based cracking catalyst, the yields of ethylene and propylene were enhanced with the increasing proportion of dehydrogenation active sites.

Table 3 The product distribution of *n*-octane dehydrogenation reaction with $CaMnO_3$@Na_2WO_4

Yields (wt%)						
Reaction temperature (°C)		500	550	600	650	700
Dry gas	Hydrogen	0.01	0.02	0.01	0.01	0.02
	Methane	0.16	0.32	0.89	1.70	2.11
	Ethane	0.22	0.47	1.32	1.92	1.26
	Ethylene	1.00	1.57	3.82	8.08	13.10
LPG	Propane	0.13	0.19	0.36	0.53	0.53
	Propylene	0.90	1.27	3.59	4.48	6.50
	n-Butane	0.15	0.23	0.51	0.41	0.22
	Isobutane	0.00	0.00	0.00	0.00	0.00
	Butylene	0.73	1.00	2.02	3.39	4.76
Gasoline product		96.71	94.93	84.76	79.49	69.89
	Octene	0.83	0.67	0.51	0.48	0.43

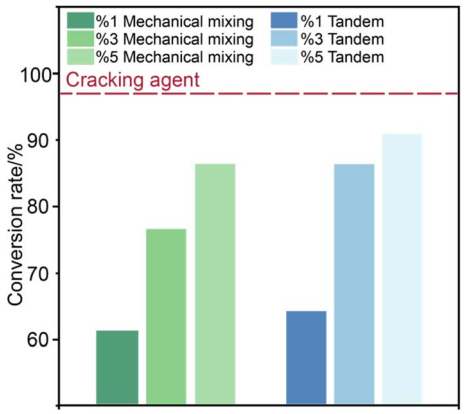

Fig. 7 Effect of different coupling methods and mixing ratios on the conversion of *n*-octane dehydrogenation cracking reaction.

With the addition of 1% perovskite dehydrogenation catalyst, the ethylene yield is 12.9%, propylene yield is 19.9%. When additional 5% perovskite dehydrogenation catalyst was physically mixed, the ethylene and propylene yields increased to 16.3% and 27.9%. The detailed product distribution was shown in Table S1.†

For tandem mixed catalysts, with the addition of 1% dehydrogenation catalyst in tandem mixing, the ethylene yield was 15.0%, propylene yield was 19.6%. With the addition of 5% perovskite dehydrogenation catalyst in tandem mixing, the ethylene and propylene yield were 20.3% and 27.6%. Comparing to standalone zeolites, 15% higher olefin yields were obtained with tandem mixed catalysts, demonstrating the excellent dehydrogenation cracking ability. Synergetic effect of zeolite catalyst with different mixing ratio of $CaMnO_3$@Na_2WO_4 also leads to tunable P/E ratio.

The combination of zeolite and $CaMnO_3$@Na_2WO_4 perovskite are bi-functional: zeolite catalyzes light alkane cracking *via* its acid sites. $CaMnO_3$@Na_2WO_4 selectively oxidizes hydrogen into H_2O, providing the heat required for *n*-octane vaporization and the endothermic cracking reactions. Meanwhile, zeolite facilitates higher *n*-octane conversions. Standalone catalytic cracking with zeolite is highly endothermic, whereas selective hydrogen combustion becomes mildly exothermic, allowing auto-thermal operation with improved overall process efficiency. Resulting from the synergistic effect between zeolite and perovskite, high single-pass olefin yield was observed along with and tunable P/E ratio.

3.5 Interplay of dehydrogenation and cracking active sites

The main challenge for the industrial dehydrogenation cracking process is that the reaction temperature of fluid catalytic cracking (FCC) is generally around 550–600 °C, which is more favorable for cracking reaction but undesirable and unsuitable for dehydrogenation elementary reaction. From the perspective of thermodynamics, the reaction equilibrium of dehydrogenation reaction was calculated in above discussion. From the above theoretical thermodynamics calculation, it could be observed that thermal cracking happened from 600 °C, and reaction rates increased above this temperature. The dehydrogenation temperature should be under 600 °C to avoid thermal cracking.

The theoretical reaction routes and kinetics of *n*-octane dehydrogenation cracking reaction were presented in Fig. 9 (Path II), compared with traditional cracking routine (Path I) as a reference. Path I indicated the reaction path of *n*-otane cracking reaction, which is an endothermic reaction. In Path II, it could be observed that the modified reaction path from octane to octene is an exothermic reaction *via* dehydrogenation. The following formation of ethylene and propylene is an endothermic reaction. It could be hypothesized that high temperature is not beneficial for the dehydrogenation elementary reaction. In our previous research, it indicated that if the

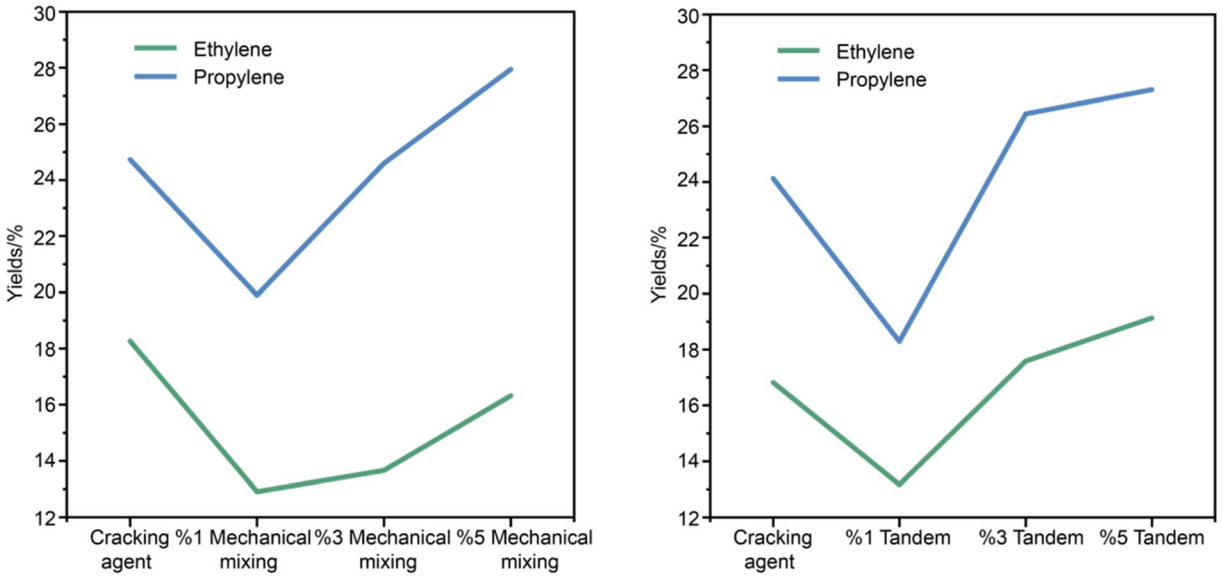

Fig. 8 Yields of ethylene and propylene in physically and tandem mixed dehydrogenation cracking reaction with mixing ratios of 1%, 3% and 5%.

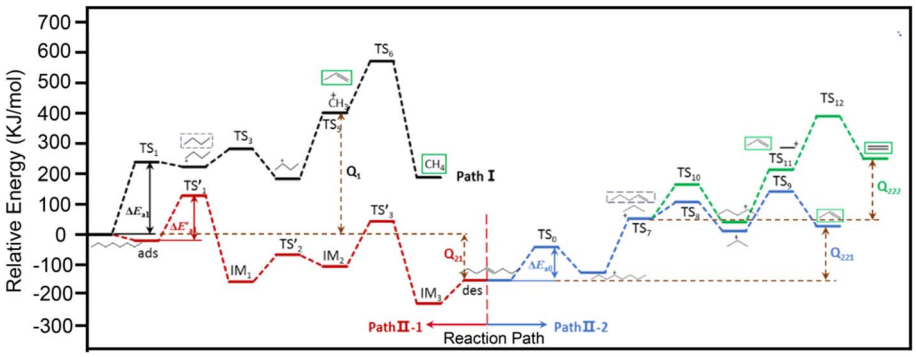

Fig. 9 The reaction routes and kinetics of *n*-octane dehydrogenation cracking reaction and standalone cracking reaction.

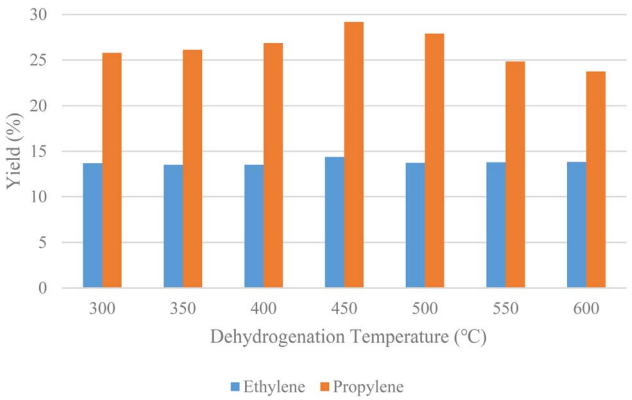

Fig. 10 Yields of ethylene and propylene with decreasing dehydrogenation temperature in tandem catalysis with mixing ratio of 2%.

reaction pathways could be modulated to convert *n*-octane to octene *via* dehydrogenation, the energy barrier would decrease. The formation of olefins can accelerate the formation of a carbenium ion and suppress the alkane intermediates, thus promoting the conversion of *n*-octane to produce light olefins.[37]

Following this hint, the dehydrogenation and cracking systems were decoupled. The cracking temperature was kept constant at 600 °C. The mixing ratio of dehydrogenation catalysts $CaMnO_3$@Na_2WO_4 in tandem catalysis was 2%. The dehydrogenation temperature was gradually decreased from 600 °C to 300 °C. As Fig. 10 shown, decreasing the dehydrogenation temperature can increase ethylene and propylene yields. Maximum yield was achieved at 450 °C. This means that by lowering the dehydrogenation temperature, we could provide an optimal reaction environment for this elementary dehydrogenation reaction and decrease the energy consumption.

4 Conclusion

In summary, we demonstrated the novel dehydrogenation cracking approach for the conversion of naphtha to light olefins. Theoretical thermodynamic analysis proposed that dehydrogenation temperature should be kept under 600 °C to avoid thermal cracking. Fixed-bed experiments are performed to prove the effectiveness of $CaMnO_3$@Na_2WO_4 for *n*-octane dehydrogenation reaction. Furthermore, tandem catalysis of $CaMnO_3$@Na_2WO_4 redox catalysts and zeolite-based catalyst exhibited satisfactory olefin yields under milder reaction conditions, establishing the feasibility of dehydrogenation cracking process in the context of olefin production. When the catalysts were coupled in tandem catalysis, the synergetic effect occurred with 5% of the dehydrogenation catalyst, achieving *n*-octane conversion of 90.07% and total light olefin yields of 47.90%, with ethylene and propylene yields of 20.30% and 27.60%, respectively. Synergetic effect of zeolite catalyst with different mixing ratio of $CaMnO_3$@Na_2WO_4 also leads to tunable P/E ratio. These findings not only provide an effective method for the production of light olefins from naphtha, but also offer insights for reactor design and optimizations of redox catalysts.

Data availability

The data that support the findings of this study are available on request from the corresponding author, upon reasonable request.

Conflicts of interest

There are no conflicts to declare.

References

1 Y. Gao, L. Neal, D. Ding, W. Wu, C. Baroi, A. M. Gaffney and F. Li, Recent advances in intensified ethylene production—a review, *ACS Catal.*, 2019, **9**(9), 8592–8621.
2 T. Xie, J. Ding, X. Shang, X. Zhang and Q. Zhong, Effective synergies in indium oxide loaded with zirconia mixed with silicoaluminophosphate molecular sieve number 34 catalysts for carbon dioxide hydrogenation to lower olefins, *J. Colloid Interface Sci.*, 2023, **635**, 148–158.
3 Y.-K. Park, C. W. Lee, N. Y. Kang, W. C. Choi, C. Sun, S. H. Oh and S. P. Deuk, Catalytic cracking of lower-valued hydrocarbons for producing light olefins, *Catal. Surv. Asia*, 2010, **14**, 75–84.
4 A. Ali, M. Nadeem, A. Naveed, J. M. Moradian, S. N.-U.-Z. Haider, S. Khan, A. M. Bhayo, *et al.*,

Copolymerization of ethylene and isoprene initiated by metallocene catalyst, *Arabian J. Chem.*, 2024, **17**(11), 105989.

5 A. Ali, J. M. Moradian, N. Ahmad, S. N.-U.-Z. Haider, J. Lu, S. S. A. Shah, H. A. Keerio, *et al.*, Capability of isoprene and butadiene as comonomers under metallocene catalysis: Activating active sites with the addition of 1-hexene and propylene, *J. Catal.*, 2024, **438**, 115729.

6 A. Ali, J. Mohammadi Moradian, N. Ahmad, S. Najeeb-Uz-Zaman Haider, W. A. Qureshi, S. Khan, H. Naz, *et al.*, To overcome the unconventional polymerization behavior of single-site symmetrical metallocene catalyst in the presence of borate, *Appl. Catal., A*, 2024, **683**, 119830.

7 A. Ali, A. Naveed, A. Maroń, M. Adnan Younis, J. Mohammadi Moradian, B. Yousaf, T. Aziz, *et al.*, Copolymerization of ethylene and isoprene *via* silicon bridge metallocene [rac-Me2Si (2-Me-4-Ph-Ind) 2ZrCl2] catalyst: A new way to control the composition and microstructure of copolymers, *Chemosphere*, 2024, **347**, 140700.

8 A. Ali, M. Nadeem, A. Naveed, T. Aziz, M. K. Tufail, J. M. Moradian, N. Ahmad, *et al.*, Ansa-metallocene catalyst based on 3-phenyl and 4-methyl substituted: catalyst evaluation in conjugated and non-conjugated diene polymerization, *J. Polym. Res.*, 2023, **30**(8), 318.

9 A. Ali, A. M. Bhayo, N. Ahmad, T. Aziz, N. Ahmad, W. A. Qureshi, A. Younis, *et al.*, Why only half of the added ansa-metallocene catalyst active in the E/P/diene polymerization: catalyst evaluation in terms of active center [Zr]/[C*] fraction and polymerization propagation rate constants, *J. Macromol. Sci., Part A: Pure Appl. Chem.*, 2023, **60**(6), 417–426.

10 A. Ali, K. F. S. Alabbosh, A. Naveed, A. Uddin, Y. Chen, T. Aziz, J. M. Moradian, *et al.*, Evaluation of the Dielectric and insulating properties of newly synthesized ethylene/1-hexene/4-Vinylcyclohexene Terpolymers, *ACS Omega*, 2022, **7**(35), 31509–31519.

11 A. Ali, J. M. Moradian, N. Ahmad, T. Aziz, N. Muhammad, C. Maouche, Y. Guo, *et al.*, Progress toward polymerization reaction monitoring with different dienes: how small amounts of dienes affect ansa-zirconocenes/borate/triisobutylaluminium catalyst systems, *Polymers*, 2022, **14**(16), 3239.

12 A. Ali, A. Naveed, K. Shehzad, T. Aziz, R. Tahir, J. M. Moradian, M. Hassan, A. Rahman, Z. Fan and L. Guo, Polymerization kinetics of bicyclic olefins and mechanism with symmetrical ansa-metallocene catalysts associated with active center count: Relationship between their activities and structure and activation path, *RSC Adv.*, 2022, **12**(24), 15284–15295.

13 Q. Shen, J. Gu, L. Shang, S. Liu, X. Song, W. Yu, Y. Liu, N. Sun and W. Wei, Carbon emissions and low-carbon development in Olefin industry, *Environ. Res.*, 2024, **244**, 117841.

14 X. Guo, X. Zhang, G. Wu, J. Gong and F. Jin, Discrimination of the Synergistic Effect of Different Zinc Active Sites with a Brønsted Acid in Zeolite for Dehydrogenation Cracking of n-Octane and Ethane Dehydroaromatization, *Langmuir*, 2024, **40**(52), 27470–27480.

15 S.-Y. Chen, Z. Qi, M. Benjamin and T.-T. Zhang, Review on the petroleum market in China: history, challenges and prospects, *Pet. Sci.*, 2020, **17**, 1779–1794.

16 X. Zhang, J. Hong, C. Zhang, Q. Liu, J. Zhang and G. Qian, Controlling effect of TiO2 carrier on formed vanadium species for effective catalytic oxidization of chlorobenzene, *Appl. Surf. Sci.*, 2022, **605**, 154643.

17 O. O. James, S. Mandal, N. Alele, B. Chowdhury and S. Maity, Lower alkanes dehydrogenation: Strategies and reaction routes to corresponding alkenes, *Fuel Process. Technol.*, 2016, **149**, 239–255.

18 S. Yusuf, L. M. Neal and L. Fanxing, Effect of promoters on manganese-containing mixed metal oxides for oxidative dehydrogenation of ethane *via* a cyclic redox scheme, *ACS Catal.*, 2017, **7**(8), 5163–5173.

19 Y. Gao, F. Haeri, F. He and F. Li, Alkali metal-promoted La x Sr2–x FeO4− δ redox catalysts for chemical looping oxidative dehydrogenation of ethane, *ACS Catal.*, 2018, **8**(3), 1757–1766.

20 N. Miura, H. Ikeda and A. Tsuchida, Sr1–x Ca x FeO3-δ as a New Oxygen Sorbent for the High-Temperature Pressure-Swing Adsorption Process, *Ind. Eng. Chem. Res.*, 2016, **55**(11), 3091–3096.

21 H. Du, H. Luo, M. Jiang, X. Yan, F. Jiang and H. Chen, A review of activating lattice oxygen of metal oxides for catalytic reactions: Reaction mechanisms, modulation strategies of activity and their practical applications, *Appl. Catal., A*, 2023, **664**, 119348.

22 L. F. de Diego, A. Abad, A. Cabello, P. Gayan, F. Garcia-Labiano and J. Adanez, Reduction and oxidation kinetics of a CaMn0. 9Mg0. 1O3− δ oxygen carrier for chemical-looping combustion, *Ind. Eng. Chem. Res.*, 2014, **53**(1), 87–103.

23 R. B. Dudek, Y. Gao, J. Zhang and F. Li, Manganese-containing redox catalysts for selective hydrogen combustion under a cyclic redox scheme, *AIChE J.*, 2018, **64**(8), 3141–3150.

24 A. Mishra, A. Shafiefarhood, J. Dou and F. Li, Rh promoted perovskites for exceptional "low temperature" methane conversion to syngas, *Catal. Today*, 2020, **350**, 149–155.

25 M. Bosomoiu, G. Bozga, D. Berger and C. Matei, Studies on combustion catalytic activity of some pure and doped lanthanum cobaltites, *Appl. Catal., B*, 2008, **84**(3–4), 758–765.

26 A. Vijay and R. Jose, Enhancement in the electrical transport properties of CaMnO 3 *via* La/Dy co-doping for improved thermoelectric performance, *RSC Adv.*, 2023, **13**(28), 19651–19660.

27 G. Saracco, F. Geobaldo and G. Baldi, Methane combustion on Mg-doped LaMnO3 perovskite catalysts, *Appl. Catal., B*, 1999, **20**(4), 277–288.

28 C.-Y. Yoo and H. J. M. Bouwmeester, Oxygen surface exchange kinetics of SrTi 1− x Fe x O 3− δ mixed conducting oxides, *Phys. Chem. Chem. Phys.*, 2012, **14**(33), 11759–11765.

29 K. Wakui, K. Satoh, G. Sawada, K. Shiozawa, K. Matano, K. Suzuki, T. Hayakawa, Y. Yoshimura, K. Murata and F. Mizukami, Dehydrogenative cracking of n-butane using

double-stage reaction, *Appl. Catal., A*, 2002, **230**(1–2), 195–202.

30 O. O. James, S. Mandal, N. Alele, B. Chowdhury and S. Maity, Lower alkanes dehydrogenation: Strategies and reaction routes to corresponding alkenes, *Fuel Process. Technol.*, 2016, **149**, 239–255.

31 J. Liang, D. Liu, S. Xu and M. Ye, Comparison of light olefins production routes in China: combining techno-economics and security analysis, *Chem. Eng. Res. Des.*, 2023, **194**, 225–241.

32 L. Dimesso, Pechini processes: an alternate approach of the sol–gel method, preparation, properties, and applications, *Handbook of Sol-Gel Science and Technology*, 2016, vol. 2, pp. 1–22.

33 S. Yusuf, L. Neal, Z. Bao, Z. Wu and F. Li, Effects of sodium and tungsten promoters on Mg6MnO8-based core–shell redox catalysts for chemical looping—Oxidative dehydrogenation of ethane, *ACS Catal.*, 2019, **9**(4), 3174–3186.

34 F. Hao, Y. Gao, L. Neal, R. B. Dudek, W. Li, C. Chung, B. Guan, P. Liu, X. Liu and F. Li, Sodium tungstate-promoted CaMnO3 as an effective, phase-transition redox catalyst for redox oxidative cracking of cyclohexane, *J. Catal.*, 2020, **385**, 213–223.

35 Y. Gao, S. Wang, H. Fang, Z. Dai and F. Li, Zeolite–perovskite composites as effective redox catalysts for autothermal cracking of n-hexane, *ACS Sustain. Chem. Eng.*, 2020, **8**(38), 14268–14273.

36 R. B. Dudek, X. Tian, M. Blivin, L. M. Neal, H. Zhao and F. Li, Perovskite oxides for redox oxidative cracking of n-hexane under a cyclic redox scheme, *Appl. Catal., B*, 2019, **246**, 30–40.

37 X. Zhang, J. Gong, X. Wei and L. Liu, Increased light olefin production by sequential dehydrogenation and cracking reactions, *Catalysts*, 2022, **12**(11), 1457.